Bulletin of Earthquake Engineering
https://doi.org/10.1007/s10518-021-01166-1

ORIGINAL ARTICLE

Analytical model for response spectral ratio considering the effect of earthquake scenarios

Haizhong Zhang[1] · Yan-Gang Zhao[1]

Received: 12 November 2020 / Accepted: 21 June 2021

Abstract
The response spectral ratio (RSR) used to construct a design spectrum that incorporates site effects is conventionally assumed to be independent of an earthquake scenario in linear analysis. However, recent studies have found that the RSR varies significantly with an earthquake scenario, even in linear analysis. In this study, an analytical RSR model that incorporates the effect of an earthquake scenario is proposed. To this end, the mechanism behind the effect of earthquake scenarios, i.e., the variation in the RSR with an earthquake scenario, is systematically investigated by comparisons with the scenario-independent Fourier spectral ratio based on random vibration theory. The proposed RSR model is verified by comparing its results with those obtained from a SHAKE analysis considering a variety of actual soil conditions. Based on the proposed RSR model, the design spectrum incorporating site effects can be reasonably and easily constructed.

Keywords Response spectral ratio · Effect of earthquake scenarios · Design spectrum · Fourier spectral ratio

1 Introduction

The ratio of the response spectrum on a ground surface to that on a reference bedrock plays an important role in the construction of a design spectrum (International Building Code (IBC) 2012; European Committee for Standardization CEN 2004; Japanese Seismic Design Code 2000). The response spectral ratio (RSR) reflects the site amplification effects on the response spectrum; by multiplying the RSR with the spectrum specified on the bedrock, a design spectrum incorporating site effects can be obtained. Many RSR models have been developed to construct a design spectrum (Borcherdt 1994; Dobry et al. 2000; Lam et al. 2001; Tsang et al. 2006, 2017; Zhang and Zhao 2018, 2019; Japanese Seismic Design Code 2000). The basic principle to develop RSR models is generally based on the Fourier spectral ratio (FSR), which categorizes the RSR into linear and nonlinear components. The nonlinear component reflects the modification of soil properties resulting from the

✉ Yan-Gang Zhao
zhao@kanagawa-u.ac.jp

1 Department of Architecture, Kanagawa University, Yokohama, Japan

Published online: 03 July 2021

nonlinear hysteretic behavior of the soil when exposed to strong levels of excitation. The linear component is from the site and independent of the earthquake scenario.

However, recent studies have found that even in linear analysis, the RSR is affected not only by the properties of soil profiles but also by those of earthquake scenarios (Zhao et al. 2009; Zhao and Zhang 2010). Bora et al. (2016) and Stafford et al. (2017) presented a theoretical explanation for this phenomenon and further pointed out that the effect of the earthquake scenario is particularly significant in very short periods. Zhang and Zhao (2021) investigated the variation in the RSR with earthquake scenarios by comparing the RSR and FSR based on statistical analyses of seismic records. Figure 1 presents a case study of an elastic single-layer soil profile on a half-space bedrock subjected to different earthquake motions. It can be observed that in contrast to the FSR, the RSR varies significantly with the input earthquake motion, even in linear analysis.

When the RSRs used for seismic design are derived based on statistical analyses of seismic records from one region and applied to this or another region with similar seismological properties (including various factors affecting characteristics of the earthquake scenario, e.g., tectonic context, source mechanisms, and attenuation), ignoring the effect of earthquake scenarios on the RSR may not have significant impacts on the design spectrum. This is because to a certain extent, the effect of earthquake scenarios in this region has been included in the statistical analysis. However, when the RSRs from a region are applied to other regions with completely different seismological properties (such applications often occur in regions with a lack of seismic records for the statistical analysis (Tsang et al. 2006)), ignoring the effect of the earthquake scenario on the RSR can lead to certain unrealistic behaviors of the design spectrum. This is because, as mentioned previously, different characteristics of the earthquake motion may lead to completely different values of the RSR.

In principle, the dependency of the RSR on earthquake scenarios can be reflected through site response analyses (Idriss and Sun 1992; Park and Hashash 2004). However, these analyses require time-history input instead of the response spectrum, which is generally not available in seismic codes. Although time histories can be generated from the bedrock spectrum, this will not only introduce more assumptions, such as the duration, envelope function, and phase angle of the ground motion, but also needs to generate a set of motions and perform many time analyses to obtain stable estimates.

In this study, a simple analytical RSR model that considers the effect of earthquake scenarios is proposed. Hence, the mechanism behind the effect of earthquake scenarios,

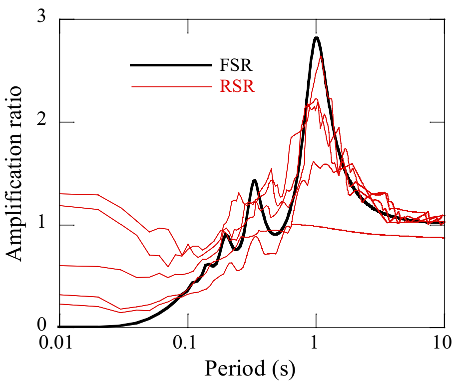

Fig. 1 Response spectral ratios for different input earthquake

i.e., the variation in the RSR with the earthquake scenario for linear analysis is systematically investigated in Sects. 2 and 3. Because the FSR is independent of the earthquake scenario for linear analysis, the effect of earthquake scenarios on the RSR is explored by comparing the RSR with the FSR based on random vibration theory (RVT). Based on this, an analytical model for the RSR that considers the effect of earthquake scenarios is presented in Sect. 4. Finally, in Sect. 5, the proposed RSR model is verified by a comparison with SHAKE analysis results while considering a variety of actual soil conditions.

2 Expression for the RSR

To develop an RSR model considering the effect of earthquake scenarios, the mechanism of the effect of earthquake scenarios, i.e., the variation in the RSR with earthquake scenarios for linear analysis should be clarified. Stafford et al. (2017) presented an approach for the analysis of the RSR based on RVT, which is efficient for solving this problem. According to the RVT, the response spectrum $R(\bar{\omega}, h_0)$ can be obtained from the zeroth moment of the Fourier amplitude spectrum (FAS) of the response of a single-degree-of-freedom (SDOF) oscillator (Boore 1983, 2003), which is expressed as

$$R(\bar{\omega}, h_0) = \frac{pf_r}{\sqrt{D_r}} \sqrt{m_{0,r}} \tag{1}$$

where $\bar{\omega}$ and h_0 are the circular frequency and damping ratio of the SDOF oscillator (hereafter referred to as the oscillator), respectively; pf_r and D_r are the peak factor and duration of the oscillator response, respectively; and $m_{0,r}$ is the zeroth moment of the FAS of the oscillator response.

Thus, the RSR can be obtained by dividing the ground-surface response spectrum by the bedrock response spectrum, which is expressed as

$$RSR(\bar{\omega}, h_0) = \sqrt{\frac{m_{0,sr}}{m_{0,br}}} \times \frac{pf_{rs}/\sqrt{D_{rs}}}{pf_{rb}/\sqrt{D_{rb}}} \tag{2}$$

where, pf_{rs} and pf_{rb} are the peak factors of the oscillator responses for the ground surface and reference bedrock motions, respectively; D_{rs} and D_{rb} are the durations of the oscillator responses for the ground surface and bedrock motions, respectively; $m_{0,sr}$ and $m_{0,br}$ denote the zeroth spectral moments of the oscillator responses for the ground surface and bedrock motions, respectively. Here, the reference bedrock motion is assumed to represent the incident motion beneath the soil profile corresponding to the ground-surface motion.

The zeroth spectral moment of the bedrock motion's oscillator response $m_{0,br}$ can be obtained from the FAS of the bedrock motion's oscillator response by

$$m_{0,br} = \frac{1}{\pi} \int_0^{\infty} \left| A_B(\omega) | H_0(\omega, \bar{\omega}, h_0) | \right|^2 d\omega \tag{3}$$

where ω is the circular frequency, $A_B(\omega)$ is the FAS of the bedrock motion, and $H_0(\omega, \bar{\omega}, h_0)$ is the SDOF transfer function, expressed as

$$\left|H_0(\omega,\bar{\omega},h_0)\right| = \frac{\bar{\omega}^2}{\sqrt{(2h_o\omega\bar{\omega})^2+(\omega^2-\bar{\omega}^2)^2}} \tag{4}$$

Similarly, the zeroth spectral moment of the ground-surface motion's oscillator response $m_{0,sr}$ can be obtained from the FAS of the ground-surface motion's oscillator response by

$$m_{0,sr} = \frac{1}{\pi}\int_0^\infty \left|A_S(\omega)|H_0(\omega,\bar{\omega},h_0)|\right|^2 d\omega \tag{5}$$

Here, $A_S(\omega)$ is the FAS of the ground-surface motion, which can be obtained from the bedrock-motion FAS via

$$A_S(\omega) = A_B(\omega)|T(\omega)| \tag{6}$$

where $T(\omega)$ is the site transfer function and $|T(\omega)|$ represents the Fourier spectral ratio (FSR) between the seismic motion on the ground surface and that on the reference bedrock. As the paper focuses on the response spectrum of acceleration, throughout the paper, the response spectra, Fourier spectra, and transfer functions are all for acceleration.

Stafford et al. (2017) assume that the peak factor and duration of the ground-surface motion's oscillator response (pf_{rs}, D_{rs}) are equal to those of the bedrock motion's oscillator response (pf_{rb}, D_{rb}), thus, Eq.(2) can be simplified as

$$\mathrm{Amp}(\bar{\omega},h_0) = \sqrt{\frac{m_{0,sr}}{m_{0,br}}} \tag{7}$$

However, many studies have reported that the duration of a seismic motion can be modified by the site response (Kottke and Rathje 2013; Wang and Rathje 2016) and then the oscillator response (Liu and Pezeshk 1999, and Boore and Thompson 2012, 2015). Thus, the duration of the ground-surface motion's oscillator response, D_{rs}, should be different from that of the bedrock motion's oscillator response, D_{rb} (Kottke and Rathje 2013; Wang and Rathje 2016). To be more precise, the effects of the duration and peak factor on the RSR are considered in this study using Eq.(2). In addition, for convenience in the following analysis, Eq. (2) is rearranged as

$$RSR(\bar{\omega},h_0) = \sqrt{\frac{\int_0^\infty W(\omega,\bar{\omega})|T(\omega)|^2 d\omega}{\int_0^\infty W(\omega,\bar{\omega})d\omega}} \times \frac{pf_{rs}/\sqrt{D_{rs}}}{pf_{rb}/\sqrt{D_{rb}}} \tag{8}$$

where $W(\omega,\bar{\omega})$ is the square of the FAS of the bedrock motion's oscillator response, expressed as

$$W(\omega,\bar{\omega}) = A_B^2(\omega)|H_0(\omega,\bar{\omega},h_0)|^2 \tag{9}$$

Many equations have been proposed for the peak factor (Cartwright and Longuet-Higgins1956; Davenport 1964; Vanmarcke 1975), among which the equation reported by Cartwright and Longuet-Higgins (1956) is commonly used in engineering seismology and site-response applications. In RVT analysis, the expected value of the peak factor is commonly used. For large numbers of extrema, the equation for the expected value of the peak factor of a seismic motion, $\bar{pf}$, reported by Cartwright and Longuet-Higgins (1956) can be simplified as

$$\bar{pf} = [2\ln(N_z)]^{1/2} + \frac{0.5772}{[2\ln(N_z)]^{1/2}} \tag{10}$$

where N_z represents the number of zero crossings, which can be expressed as

$$N_z = \frac{1}{\pi}\sqrt{\frac{m_2}{m_0}} \tag{11}$$

Here, m_0 and m_2 are the zeroth and second moments of the FAS of the seismic motion, respectively.

3 Investigating the effect of earthquake scenarios

This section explores the effect of earthquake scenarios on the RSR using Eq. (8). Equation (8) is the product of two terms: the first term is determined by $|T(\omega)|^2$ and $W(\omega, \bar{\omega})$, and the second term is determined by the durations and peak factors. The characteristics of these two terms are investigated in the following two sections. Then, the effect of earthquake scenarios on the RSR is discussed according to the characteristics. Because the RSR and FSR are often used to characterize site effects, and the FSR is independent of the earthquake scenario for linear analysis, the effect of earthquake scenarios on the RSR is explored by comparing the two spectral ratios. Although the FSR, $T(\omega)$, and RSR are functions of circular frequency, the two frequencies are physically different: the FSR one ω is the circular frequency of the seismic motion's FAS, whereas the RSR one $\bar{\omega}$ is the oscillator circular frequency.

3.1 Characteristics of the first term

3.1.1 Mathematical considerations

To investigate the first term, its mathematical characteristics are analyzed. It is found that the part under the radical sign of the first term represents a weighted average of the values of $|T(\omega)|^2$, with $W(\omega, \bar{\omega})$ acting as the weight function. The value of the square of the first term at any circular oscillator frequency $\bar{\omega}$ equals the weighted average of all values of $|T(\omega)|^2$ at frequencies from zero to infinity (Hz), and the weight $W(\omega, \bar{\omega})$ is distributed as a function of the circular frequency ω. For values of the first term at different circular oscillator frequencies, Eq. (9) shows that the weight function $W(\omega, \bar{\omega})$ varies with the oscillator frequency $\bar{\omega}$. Equation (9) indicates that the weight function $W(\omega, \bar{\omega})$ further varies with the FAS of the bedrock motion $A_B(\omega)$. Figure 2 illustrates calculating the square of the first term at a circular oscillator frequency $\bar{\omega}$. The weighted average is used to investigate the characteristics of the first term as described in the further subsections.

3.1.2 Weight function

In the calculation of the weighted average, i.e., the first term, the weight function $W(\omega, \bar{\omega})$ plays a critical role; thus, its characteristics are investigated in this section. According to Eq. (9), $W(\omega, \bar{\omega})$ equals the product of $|H_0(\omega, \bar{\omega}, h_0)|^2$ and ${A_B}^2(\omega)$. Figure 3a indicates that the SDOF transfer function $|H_0(\omega, \bar{\omega}, h_0)|$ ($h_0 = 5\%$ in this study) conventionally has

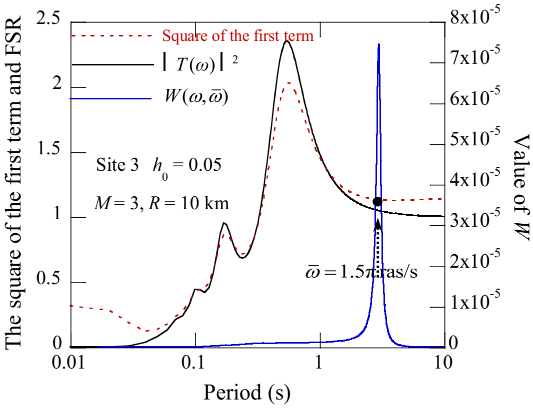

Fig. 2 Calculating the square of the first term at a circular oscillator frequency $\bar{\omega}$

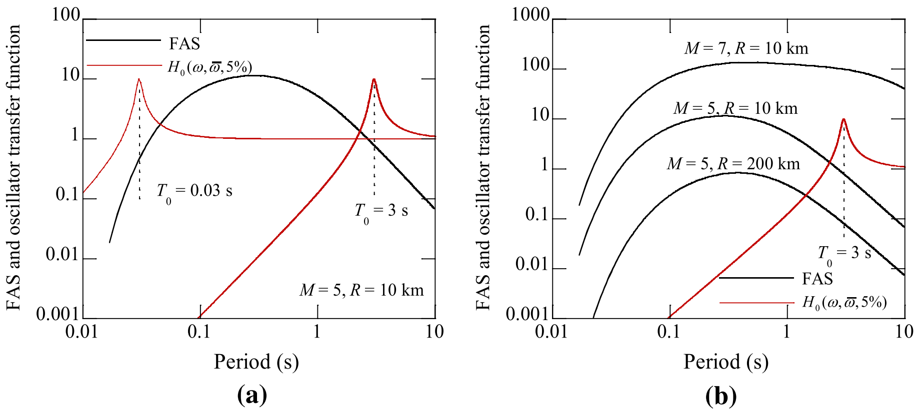

Fig. 3 Effect of **a** the oscillator period and **b** the earthquake scenario on the weight function $W(\omega, \bar{\omega})$

a narrow-band peak at the oscillator period T_o ($T_o = 2\pi/\bar{\omega}$), and decreases rapidly to zero and unity as the period decreases and increases, respectively. Thus, multiplying $A_B{}^2(\omega)$ by $|H_0(\omega, \bar{\omega}, h_0)|^2$ generally results in very large values at periods around T_o and small values at longer and shorter periods. This implies that the bandwidth of the weight function $W(\omega, \bar{\omega})$ is generally very narrow, with main weights concentrated around the oscillator period T_o, as shown in Fig. 2. However, when the oscillator period T_o is very short, the situation is very different. As illustrated in Fig. 3a, with decreasing oscillator period T_o, the region of $|H_0(\omega, \bar{\omega}, h_0)|$ with values near unity (periods longer than T_o) increases, the weight function $W(\omega, \bar{\omega})$ becomes approximately equal to $A_B{}^2(\omega)$ at a wide range of periods longer than T_o. When the oscillator period T_o is decreased to zero, $|H_0(\omega, \bar{\omega}, h_0)|$ equals unity at all periods, and the weight function $W(\omega, \bar{\omega})$ becomes equal to $A_B{}^2(\omega)$. Therefore, when the oscillator period T_o is very short, the bandwidth of the weight function $W(\omega, \bar{\omega})$ is similar to that of $A_B(\omega)$ with weights distributed over a broad range of periods.

To demonstrate these characteristics of the weight function, several calculations were conducted considering three levels of bedrock motion with $M = 3$, $R = 10$ km, $M = 5$, $R = 10$ km, and $M = 5$, $R = 200$ km, and two oscillator frequencies. The FAS of the input bedrock motion for the analyses was generated by the Stochastic-Method SIMulation

Table 1 Parameters used in generating the FAS of the rock motion

Parameter	Value
Source spectrum	Brune ω-squared point source
Stress drop $\Delta\sigma$ (bar)	100
Site diminution k (s)	0.04
Density of crust ρ (g/ cm^3)	2.8
Shear-wave velocity of crust β (km/s)	3.7
Crust amplification	Boore and Joyner (1997) Generic Rock
Geometrical spreading	Atkinson and Boore (1995) and Frankel et al. (1996)
Path attenuation	$Q = 680f^{0.38}$

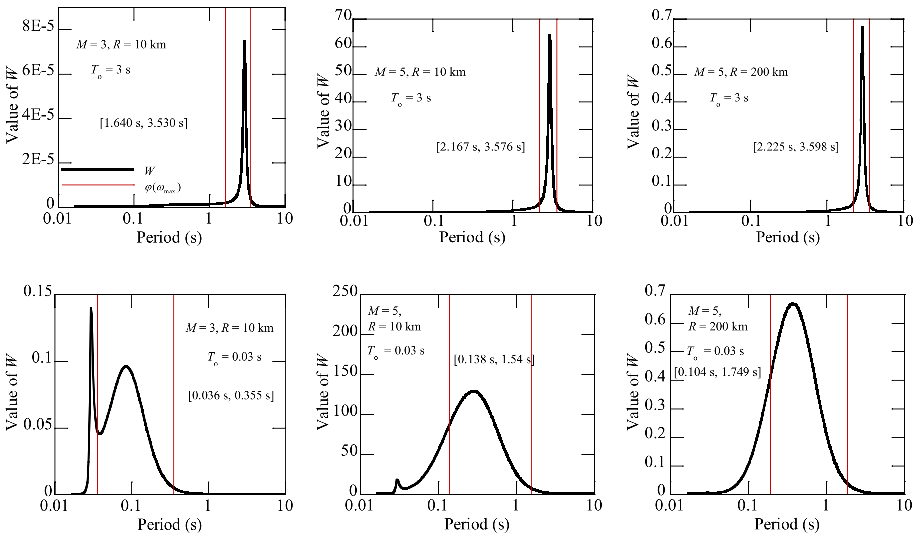

Fig. 4 Dependence of the weight function on the oscillator frequency, magnitude, and distance. The rows from top to bottom correspond to oscillator periods of T_o = 3 and 0.03 s, respectively. The columns from left to right correspond to magnitude and distance of M = 3, R = 10 km, M = 5, R = 10 km, and M = 5, R = 200 km, respectively

(SMSIM) program (Boore 2005). The important seismological parameters used to define the FAS were determined according to Boore (2003) and summarized in Table 1. The results obtained are shown in Fig. 4. In addition, to quantify the bandwidth of the weight function, a parameter $\varphi(\omega_{max})$ reported by Bora et al. (2016) is used

$$\varphi(\omega_{max}) = \frac{\int_0^{\omega_{max}} W(\omega, \bar{\omega})d\omega}{\int_0^{\infty} W(\omega, \bar{\omega})d\omega} \tag{12}$$

Periods corresponding to $\varphi(\omega_{max})$ = 0.05 and 0.95 are shown in Fig. 4. Here, ω_{max} is the upper circular frequency used in the integration. The interval of the two periods can be used to represent the bandwidth of the weight function. The results in Fig. 4 support that for the long oscillator period (T_o = 3 s), the bandwidth of the weight function is very narrow with the main weights concentrated around the oscillator period, and for the very short oscillator period ($T_o = 0.03$ s), the bandwidth widens with weights distributed over a broad range of periods.

As discussed previously, the weight function $W(\omega, \bar{\omega})$ is also affected by the FAS of the bedrock motion. When the bedrock-motion FAS changes, the distribution of the weight with the circular frequency changes. The FAS increases with an increase in magnitude, and the long-period components generally increase more than the short-period components, as shown in Fig. 3b. The FAS decreases with increasing distance, and the long-period components generally decrease less than the short-period components, as shown in Fig. 3b. Therefore, at long oscillator periods, the weights at periods around T_o increase relative to those at short periods with increasing magnitude and distance. This means that the weight concentrates at the oscillator period T_o with increasing magnitude and distance. This conclusion is demonstrated in Fig. 4, which shows that for long oscillator periods, the bandwidth of the weight function decreases with increasing magnitude and distance. However, when the oscillator period is very short, because the weight function $W(\omega, \bar{\omega})$ is dominated by ${A_B}^2(\omega)$ and the period band of $A_B(\omega)$ increases with increasing magnitude and distance (Fig. 3b), the weights distribute over a broader range of periods. This conclusion is demonstrated in Fig. 4, which shows that at short oscillator periods, the bandwidth of the weight function increases with increasing magnitude and distance.

3.1.3 Conclusions based on the weighted average

Based on weighted average and properties of the weight function, the characteristics of the first term can be understood. The value of the square of the first term at any circular oscillator frequency $\bar{\omega}$ equals the weighted average of values of $|T(\omega)|^2$ at frequencies from zero to infinity (Hz). As the weighted average of a set of values cannot exceed their maximum value or decrease than their minimum value, every value of the square of the first term is smaller than the maximum value of $|T(\omega)|^2$ and larger than the minimum value of $|T(\omega)|^2$. Therefore, every value of the first term is smaller than the maximum value of $|T(\omega)|$ and larger than the minimum value of $|T(\omega)|$. The minimum value of $|T(\omega)|$ equals zero when the period approaches zero. It worth emphasizing again that $|T(\omega)|$ represents the FSR. These properties imply that the maximum value of the first term is consistently smaller than that of the FSR, and the value of the first term always exceeds zero and differs from that of the FSR in the short-period band.

To demonstrate the characteristics of the first term, simple cases of a soil layer with a constant velocity underlain by a rock half-space are considered. The thickness H of the soil layer and shear-wave velocity of the rock half-space V_B are varied, as summarized in Table 2. The shear-wave velocity of the soil layer V_S was set as 300 m/s, and the damping ratio h was set as 0.1 for the soil layer and 0 for the bedrock. Ten soil profiles were created and named as sites 1–10, as listed in Table 2. The impedance ratio a of soil layer to

Table 2 Characteristics of the created sites

Name	Site 1	Site 2	Site 3	Site 4	Site 5	Site 6	Site 7	Site 8	Site 9	Site 10
H (m)	7.5	15	37.5	75	150	7.5	15	37.5	75	150
V_s (m/s)	300									
V_B (m/s)	600					1500				

rock layer is 0.5 for sites 1–5 and 0.2 for sites 6–10. The undamped fundamental period T_1 of the sites ranges from 0.1 s for the shallowest site to 2 s for the deepest site. In addition, five levels of input bedrock motions with $M=3$, $R=10$ km, $M=5$, $R=10$ km, $M=7$, $R=10$ km, $M=5$, $R=100$ km, and $M=5$, $R=200$ km were considered. The first term of each soil profile is estimated for all considered FASs of the input bedrock motion. Then, the calculated results for the first term are compared with those for the FSR at the same frequency values. Comparisons of the results using site 8 as a representative are shown in Fig. 5. Comparisons of the first term and FSR for all sites support that the maximum value of the first term is consistently smaller than that of the FSR, and the value of the first term differs from that of the FSR in the short-period band.

In addition, while calculating the value of the first term at long oscillator periods, because the weight for the value of $|T(\omega)|^2$ at the oscillator period T_o is much larger than those for values at other periods, the value of the first term (weighted average of the values of $|T(\omega)|^2$) at an oscillator period T_o is dominated by values of $|T(\omega)|$ around the oscillator period T_o, as illustrated in Fig. 2. Therefore, the first term is similar to the FSR at long oscillator periods. Further, the overall shapes of the first term and FSR are similar, and they reach their maximum values at the same period, as shown in Fig. 5. However, while calculating the value of the first term at very short oscillator periods, because the weights are distributed over a broad range of periods, the value of the first term (weighted average of the values of $|T(\omega)|^2$) at an oscillator period is controlled by values of $|T(\omega)|$ over a broad range of periods. Therefore, the first term is very different from the FSR at short oscillator periods, as shown in Fig. 5. This was also reported by Bora et al. (2016) and Stafford et al. (2017).

Moreover, at long oscillator periods, because the bandwidth of the weight function decreases with increasing magnitude and distance, the value of the first term at an oscillator period is further affected by the value of $|T(\omega)|$ at the same period. Therefore, the value of the first term gradually approaches that of the FSR with increasing magnitude and distance at long oscillator periods, as shown in Fig. 5. For short oscillator periods, because the bandwidth of the weight function increases with increasing magnitude and distance, the value of the first term is affected by values of $|T(\omega)|$ at a wider range of periods. Therefore, the difference in values of the first term and FSR at very short oscillator periods tends to

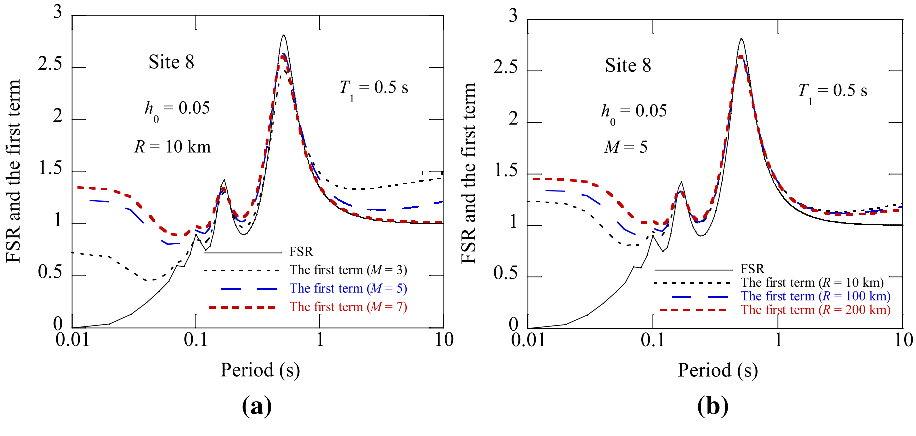

Fig. 5 Variation in the first term with **a** magnitude and **b** distance of the earthquake scenario for site 8

increase with increasing magnitude and distance, as shown in Fig. 5. In addition, it is noted that the first term varies more significantly with magnitude than distance. At 0.03 and 3 s, the average rates of change of the first term with magnitude are 18% and 7.6%, respectively, while those with distance are only 0.15% and 0.0013%, respectively.

Further identifying the key factor governing the effect of earthquake scenarios on the first term is helpful. Equations (8) and (9) show that the earthquake affects the first term by changing the weighted function. In addition, the results of the weighted average, i.e., first term, are determined by the distribution of the weight function with the circular frequency ω instead of its absolute values. Because the shape of the ground-motion FAS changes the distribution of the weight function, the effect of earthquake scenarios on the first term is governed by the shape of the ground-motion FAS. The shape of the ground-motion FAS represents the frequency content of the ground motion; therefore, the effect of the earthquake scenario on the first term is governed by the ground-motion frequency content.

3.2 Characteristics of the second term

To investigate the characteristics of the second term, the second term in Eq. (8) is analyzed. The second term can be considered as the product of pf_{rs}/pf_{rb} and $\sqrt{D_{rb}/D_{rs}}$, which represent the rates of change of the peak factor and duration of the oscillator response generated by the site response, respectively. Generally, the peak factor varies little with the affected parameters. The variation in the peak factor $\bar{pf}$ with the number of zero crossings N_z is estimated using Eq. (10). It is found that when the value of N_z varies from 20 to 1,000, the value of $\bar{pf}$ changes by only 1.74, and the average rate of change of $\bar{pf}$ with N_z is only 0.0175%. This means that even when the site response changes N_z appreciably, the change in $\bar{pf}$ is small, and thus, pf_{rs}/pf_{rb} is generally near unity. Representative results for pf_{rs}/pf_{rb} for site 8 estimated using Eq. (10) are shown in Fig. 6. It is found that all values of pf_{rs}/pf_{rb} are around unity and become closer to unity with increasing magnitude and distance. Therefore, the second term is dominated by the duration part, $\sqrt{D_{rb}/D_{rs}}$.

The duration ratio D_{rs}/D_{rb} was calculated for a range of site conditions and input motions in previous studies (Kottke and Rathje 2013; Wang and Rathje 2016). Because the second term is inversely proportional to D_{rs}/D_{rb}, using the characteristics of the duration ratio D_{rs}/D_{rb} derived in the previous studies, the characteristics of the second term can be understood. Previous studies found that the shape of D_{rs}/D_{rb} is very similar

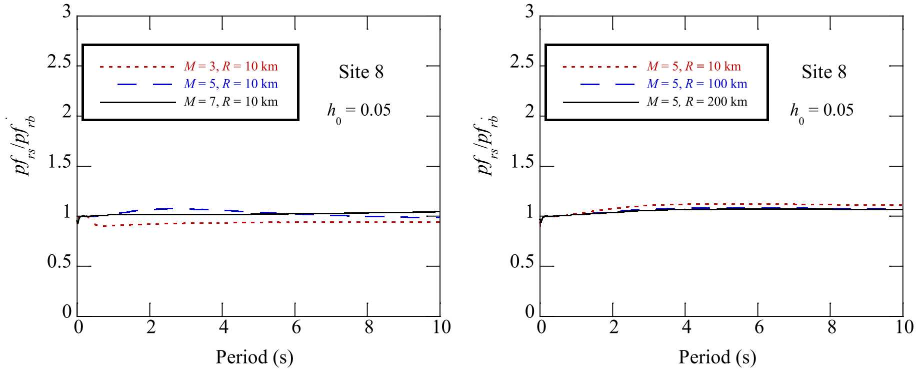

Fig. 6 Rate of change of peak factor of oscillator response generated by site response

to that of the FSR, and their peaks occur at the same site's natural periods (Kottke and Rathje 2013). This implies that the minimum valley value of the second term and maximum value of the FSR occur at the same period. In addition, it was found that the duration of the oscillator response at the fundamental period is generally extended by site response (Wang and Rathje 2016); the peak value of D_{rs}/D_{rb} at the fundamental period are always greater than unity. This implies that the minimum valley value of the second term is consistently smaller than unity. Moreover, the peak value of D_{rs}/D_{rb} at the fundamental period was found to decrease to unity with increasing magnitude (Wang and Rathje 2016). This implies that the minimum valley value increases to unity with increasing magnitude.

To demonstrate the characteristics of the second term, further analyses were conducted for the series of site conditions and input motions considered above. To accurately obtain the values of the second term, the second term is estimated using time-history analysis by the program Strata (Kottke and Rathje 2008), which has been widely used as a reference to calibrate the RVT-based analyses. The input time histories for the time-history analysis are generated from the FAS by the program SMSIM (Boore 2005) using stochastic simulation (Boore 1983). According to Atkinson and Silva (2000), the duration D_{gm} of the time history is determined using $D_{gm} = 1/f_0+0.05R$, where f_0 is the corner frequency representing the frequency below which the FAS decays. For each FSA, a suite of 100 time histories is generated, and the simulated time histories match the FAS on average.

Then, the surface response spectral accelerations of each soil profile for all the generated time histories were calculated. For each magnitude, the 100 corresponding bedrock response spectra and surface response spectra of each soil profile were averaged. The RSR is obtained as the ratio of the average surface response spectrum to the average bedrock response spectrum. Subsequently, using Eq. (8), the values of the second term are obtained as the quotient of the RSR to the first term obtained above. Representative results and their corresponding FSRs for the second term of site 8 are shown in Fig. 7. All comparisons of the second term and FSR support that the minimum valley value of the second term is consistently smaller than unity and increases to unity with increasing magnitude. In addition, it was found that the shapes of the second term are much flatter when compared with those of the FSR, all values of the second term approach unity, and the shape of the second term tends to flatten with increasing magnitude and distance.

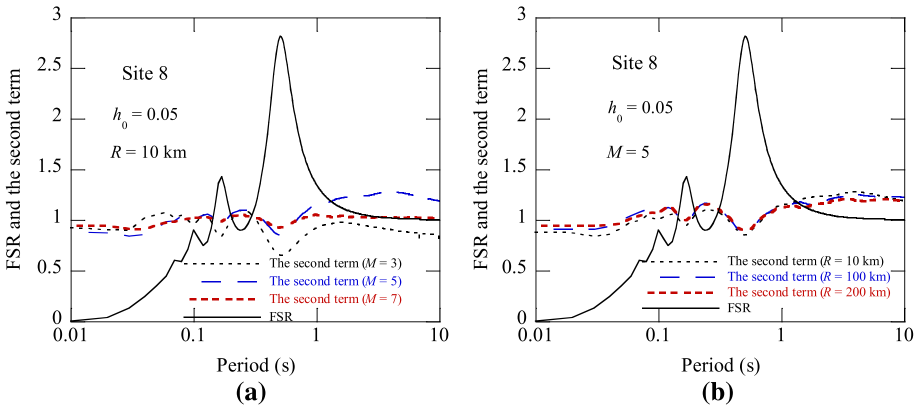

Fig. 7 Variation in the second term with **a** magnitude and **b** distance of the earthquake scenario for site 8

3.3 Characteristics of the effect of earthquake scenarios on the RSR

Based on the characteristics of the first and second terms established in the previous two sections, the characteristics of the effect of earthquake scenarios on the RSR are discussed in this section.

According to the characteristics: (1) at long periods, the values of the first term gradually approach those of the FSR with increasing magnitude and distance, and (2) the values of the second term approach unity, and the shape of the second term tends to flatten with increasing magnitude and distance. It can be inferred that the values of the RSR at long periods gradually approach those of the FSR with increasing magnitude and distance. The values of the RSR obtained above are compared with those of the FSR, and representative comparisons for site 8 are presented in Fig. 8, all results support this inference.

According to the characteristics: (1) the maximum values of the first term and FSR occur at the same period, and the maximum value of the first term is consistently smaller than that of the FSR, and (2) the minimum valley value of the second term and maximum value of the FSR occur at the same period while the minimum valley value of the second term is consistently less than unity. It can be inferred that the maximum value of the RSR should be consistently smaller than that of the FSR. This is reported in Fig. 8 and previous statistical analyses (Rosenblueth and Arciniega 1992; Zhang and Zhao 2021).

According to the characteristics: (1) the overall shape of the first term is similar to that of the FSR and the maximum values of the first term and FSR occur at the same period, and (2) the shape of the second term is much flatter when compared with that of the FSR, and all values of the second term are approximately unity. Hence, it can be inferred that the overall shape of the RSR should be similar to that of the FSR, and the maximum values of the RSR and FSR should occur at the same period, as shown in Fig. 8. This conclusion is consistent with that based on statistical analysis (Dobry 1991; Zhang and Zhao 2021).

According to the characteristics: (1) the values of the first term and FSR in the short-period band are very different, and the difference tends to increase with increasing

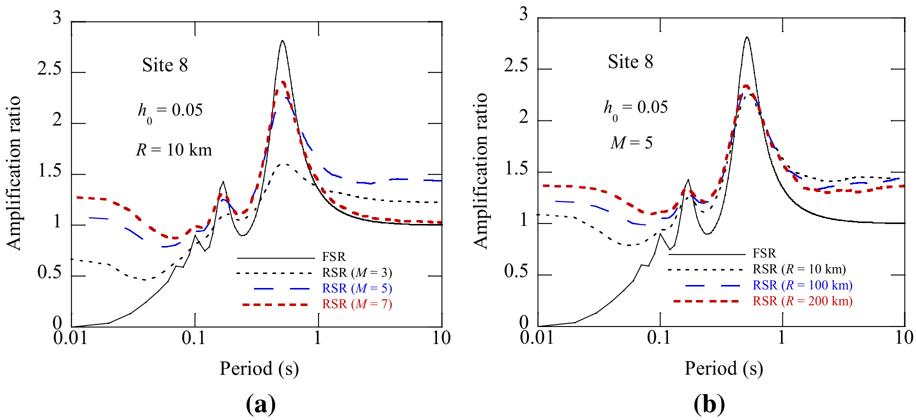

Fig. 8 Variation in the RSR with **a** magnitude and **b** distance of the earthquake scenario for site 8

magnitude and distance, and (2) all the values of the second term approach unity with increasing magnitude and distance. It can be inferred that the values of the RSR and FSR in the short-period band are different, and the difference tends to increase with increasing magnitude and distance, as shown in Fig. 8.

Moreover, according to the characteristics: (1) the effect of earthquake scenarios on the first term is governed by the ground-motion frequency content, and (2) the effect of earthquake scenarios on the second term is much smaller than that on the first term (at 0.03 and 3 s, the average rates of change of the first term with magnitude are 18% and 7.6%, respectively, while the average rates of change of the second term with magnitude are only 0.22% and 2.3%, respectively). It can be inferred that the effect of earthquake scenarios on the RSR is governed by the ground-motion frequency content.

3.4 Effect of earthquake scenarios in seismic design

This section further investigates the importance of the effect of earthquake scenarios on the RSR in practical seismic design. Hence, nonlinear site response analyses of an actual soft soil site considering two different bedrock spectra defined in the ASCE/SEI 7-10 (2011) were performed. The two bedrock spectra are shown in Fig. 9a), and the shear-wave velocity profile of the soil site is shown in Fig. 12e. The SHAKE program (Idriss and Sun 1992) is adopted for the nonlinear site response analysis. Because the SHAKE requires time-history inputs, time histories are generated from the bedrock spectrum using the software ARTEQ (Kozo Keikaku Engineering Inc.). To obtain reliable results, 10 time histories were generated for each bedrock spectrum. Then the time-history response is obtained at the ground surface based on the frequency-domain analysis of SHAKE, and then its response spectrum can be obtained. It can be observed from Fig. 9b that the average RSRs for the two bedrock spectra are significantly different, particularly in short periods. The difference may be caused by the effect of earthquake scenarios or the difference in the degree of soil nonlinearity induced by the two spectra. Figure 9c shows that the FSRs are approximately equal for the two bedrock spectra, i.e., the degree of soil nonlinearity induced by the two spectra is approximately equal. Therefore, the effect of earthquake scenarios on the RSR is important even for practical seismic design that considers soil nonlinearity.

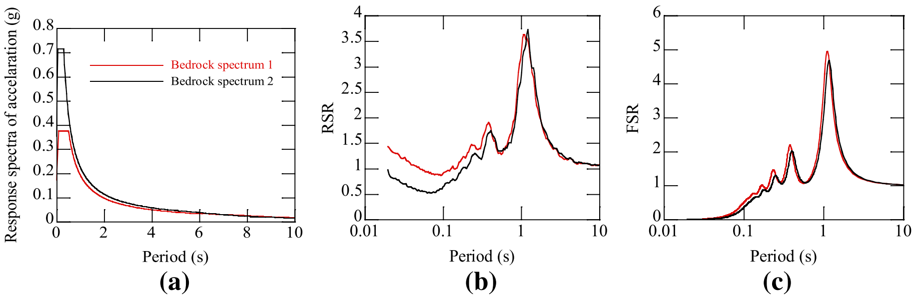

Fig. 9 Effect of earthquake scenarios in practical seismic design **a** two bedrock spectra in ASCE/SEI 7-10 (2011), **b** RSR results for the two bedrock spectra, and **c** FSR results for the two bedrock spectra

4 Analytical RSR model considering the effect of earthquake scenarios

In this section, an analytical model for the RSR considering the effect of earthquake scenarios is developed. According to the discussions in Sect. 3, to consider the effect of earthquake scenarios, the parameters determining the earthquake scenario, such as magnitude and distance, should be incorporated in the RSR model. However, because these parameters are generally not available in seismic codes, while adopting response spectrum as the seismic load, explicitly incorporating them in the RSR model is unrealistic for seismic design. The discussions in Sect. 3 indicate that although the RSR varies with the earthquake motion, the RSR is related to the scenario-independent FSR. This study attempts to incorporate the effect of earthquake scenarios into the RSR model based on these regular relationships.

4.1 Proposed RSR model

According to Sect. 3, (1) the overall shape of the RSR is similar to that of the FSR, (2) for a wide range of long periods, values of the RSR are similar to those of the FSR, and (3) when the magnitude and distance of the earthquake motion increase, the values of the RSR become approximately equal to those of the FSR, particularly for long periods. Because the design response spectrum generally corresponds to a relatively large magnitude and far distance, the design values of the RSR can be determined based on the scenario-independent FSR at most long periods. In addition, because the maximum values of the RSR and FSR occur at the same site fundamental period, and the FSR values consistently exceed the RSR values, the authors suggest using the maximum of the FSR as the design value for that of the RSR to ensure a conservative design for any input earthquake. However, at very short periods, because the two spectral ratios are different, the RSR cannot be determined with a similar approach. However, because the RSR at the period of zero equals the site amplification ratio for the peak acceleration (RPA), the RSRs in the short-period band can be estimated using the RPA. Based on these characteristics, a simple model for the RSR is proposed as

$$RSR(T_o) = \begin{cases} (RF_{T_1} - RPA)\left[\left(\frac{T_o}{T_1}\right)^{1.5} - 1\right] + RF_{T_1} & T_o \le T_1 \\ RF_{T_1} & T_1 < T_o \le 1.1T_1 \\ (RF_{T_1} - 1)\left[\left(\frac{1.1T_1}{T_o}\right)^{1.5} - 1\right] + RF_{T_1} & 1.1T_1 < T_o \end{cases} \tag{13}$$

where T_1 and RF_{T_1} represent the site fundamental period and corresponding maximum value of the FSR, respectively.

Figure 10 presents an illustration of the proposed RSR model. The RSR model is controlled by two critical points, viz. RF_{T_1} and RPA, which can be easily determined. RF_{T_1} and T_1 can be obtained using the following well-known equations (Zhang and Zhao 2018)

$$RF_{T_1} = \frac{1}{1.57h + a} \tag{14}$$

$$T_1 = \frac{4H}{V_s} \tag{15}$$

where a is the impedance ratio of the soil layer to the rock layer, and h is the soil damping ratio. The equation for the RPA is discussed in the following section. The overall function

Fig. 10 Proposed model for the RSR

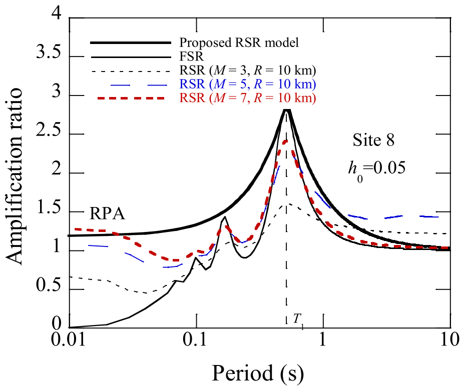

form of the RSR model is determined by trying a large number of functions while considering a balance between the simplicity and accuracy. The accuracy of the proposed model is quantified by the average relative error of the RSRs at periods from 0 to 10 s. The RSR model envelops the FSR and RPA at long and very short periods and satisfies the boundary conditions that the value decreases to the RPA and unity when the period T_0 approaches zero and infinity, respectively. In addition, the effect of the soil damping ratio on the site fundamental period is also considered in the RSR model by setting a platform from T_1 to 1.1 T_1, as shown in Fig. 10.

Equations (14) and (15) are developed based on a single-layer soil profile on the bedrock. For multi-layer soil profiles on bedrock, the multiple soil layers can be replaced by an equivalent single layer by weighted averaging the shear-wave velocity V_i of each soil layer,

$$V_s = \frac{\sum_{i=1}^{n} V_i H_i}{H} \tag{16}$$

or using the more accurate method developed by Zhang and Zhao (2018). Here, H_i represents the thickness of each soil layer. In addition, the soil nonlinear behavior, including the degradation of the shear-wave velocity and increase in the soil damping ratio, can be considered using the method reported by Inoue et al. (2010) and Tsang et al. (2006). The RSR can be easily constructed using the proposed model. Then, by multiplying the bedrock response spectrum defined in seismic codes or generated using ground motion prediction models, the design spectrum can be obtained.

When applying the proposed model in seismic design, engineers need to be aware of the conservatism incorporated in the model, i.e., using the maximum of the FSR as the design value for that of the RSR, to avoid adding unnecessary conservatism.

4.2 Simple equation for the RPA

To obtain the RSR using Eq. (13), the RPA should be determined. This section presents a simple equation for the estimation of RPA. Because the RSR at the period of zero equals the RPA, according to Eq. (8), the RPA can be expressed as

$$\mathrm{RPA} = \sqrt{\frac{\int_0^\infty A_B^2(\omega)|T(\omega)|^2 d\omega}{\int_0^\infty A_B^2(\omega)d\omega}} \times \frac{pf_s/\sqrt{D_s}}{pf_b/\sqrt{D_b}} \tag{17}$$

where D_b and pf_b represent the duration and peak factor for the bedrock motion, respectively, and D_s and pf_s represent the duration and peak factor for the ground-surface motion, respectively.

By comparing the results in Sects. 3.1 and 3.2, it is found that Eq. (8) is dominated by the first term. Thus, it can be inferred that Eq. (17) is also dominated by the first term. Based on the mathematical characteristics of the first term, the square of the RPA can be considered as a weighted average of the values of $|T(\omega)|^2$, and the square of the FAS of the bedrock motion, $A_B^2(\omega)$, acts as the weight function. The weighted average value of $|T(\omega)|^2$ must lie between the maximum and minimum values of $|T(\omega)|^2$ and equal to the value of $|T(\omega)|^2$ at a certain period T_F. This means that the RPA equals the value of $|T(\omega)|$ at a period T_F. Generally, $|T(\omega)|$ varies significantly with the period owing to the resonance effect, and it was found that using an equation for the average of $|T(\omega)|$ derived by Stafford et al. (2017) can obtain a better estimation of the RPA than using the equation of $|T(\omega)|$. Thus, the RPA is expressed as

$$\mathrm{RPA} = \frac{2}{1+a} \exp\left(-\frac{\pi}{2}\frac{T_1}{T_F}h\right) \tag{18}$$

To incorporate this equation in seismic design, an empirical equation is developed to relate the period T_F to a period T_P corresponding to the peak value of the bedrock spectrum. The RPAs of the ten soil profiles considering the five levels of bedrock motions in Sect. 3 were analyzed using the SHAKE program, and an equation, $T_F = 1.5T_P$, is regressed for Eq. (18) to yield a best prediction of the RPA, as shown in Fig. 11a. Ten time histories were generated for each FAS by the program SMSIM (Boore 2005) for the SHAKE analysis. The average value of RPAs for each FAS is used for the regression in Fig. 11a. Equation (18) is further verified using two levels of bedrock spectra defined in the Japanese Seismic Design Code (2000). Figure 11b shows that Eq. (10) can provide a very good prediction of the RPA for the bedrock spectra in the Japanese Seismic Design Code (2000).

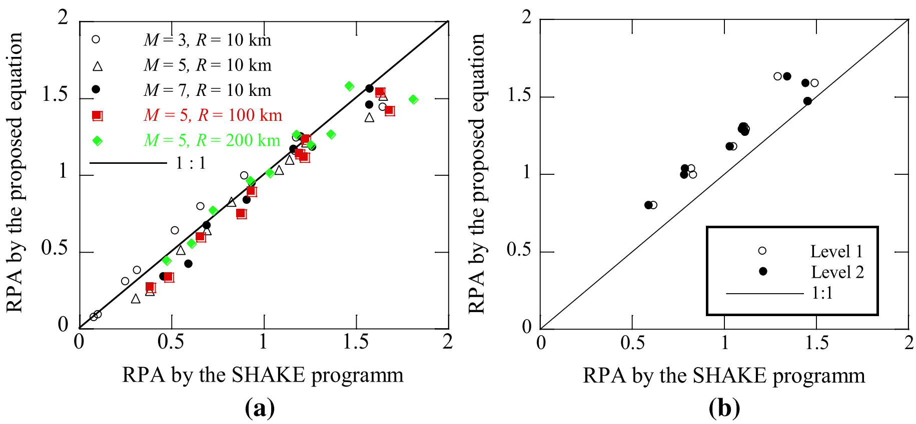

Fig. 11 Comparison of results of the RPA calculated by the proposed equation and SHAKE program using the bedrock spectra **a** used in Sect. 3, and **b** defined in Japanese Seismic Design Code

Here, T_P corresponds to the mean value of the first and second corner periods corresponding to the start and end of the acceleration plateau. Similarly, for the SHAKE analysis in Fig. 11b, 10 time histories for each response spectrum were generated, and the average value of RPAs for each response spectrum was used for comparison.

5 Verification of the proposed model

In this section, the proposed model for the estimation of the RSR is verified. Hence, a variety of actual multi-layer soil sites in Japan are used; they are named as sites 11–18, and their shear-wave-velocity profiles are presented in Fig. 12. Since shear-wave-velocity profiles beyond 30 m can also significantly affect the site response (Régnier et al. 2014), soil profiles with a variety of depths and shear-wave velocities of the bedrock are selected. The depth to the bedrock varies from 17.6 to 150 m, shear-wave velocity of the bedrock varies from 350 m/s to 2900 m/s. The shear-wave velocity of the soil varies from 80 to 390 m/s, and two sites with shear-wave velocity inversions (Fig. 12b, f) are included. Sites 11–14 are obtained from Koyamada et al. (2004), and their soil nonlinear properties were obtained by laboratory experiments using natural soil samples. Sites 15–18 are selected from strong-motion seismograph networks (K-NET, KIK-net) of Japan, and their soil nonlinear

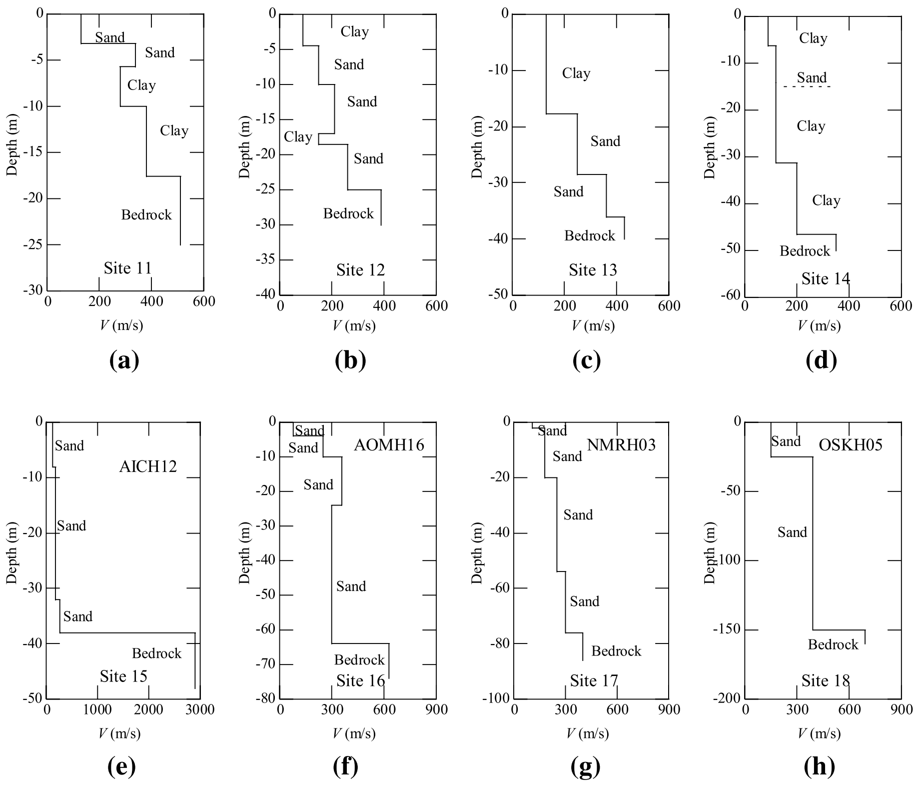

Fig. 12 Shear-wave-velocity profiles of eight actual soil sites in Japan **a** site 11, **b** site 12, **c** site 13, **d** site 14, **e** site 15, **f** site 16, **g** site 17, and **h** site 18

properties are determined empirically based on the Japanese Seismic Design Code (2000). The station codes of the four sites are presented in Fig. 12. Then, the response spectra of the eight soil sites were calculated using the proposed model and SHAKE program. The level-2 bedrock spectrum in the Japanese Seismic Design Code (2000) was used as the seismic input. The SHAKE analysis was conducted using ten spectrum-compatible time histories generated from the bedrock spectrum. The soil nonlinear behavior, including the degradation of the shear-wave velocity and increase in the soil damping ratio, are estimated using the method of Inoue et al. (2010). Then, the soil spectra obtained by the proposed model are compared with the soil spectra obtained by the SHAKE program, as shown in Fig. 13. It is found that the proposed model can provide very good estimations for most of these actual multi-layer soil sites. Although the proposed model may underestimate/overestimate the results at some periods, it can provide a very good estimation of the results at most periods. To quantify the average error at different periods, the relative error of the area of the response spectrum enclosed by the period axis (from zero to 10 s) is adopted. For most soil sites, the relative error is smaller than 5%, for one soil site with the longest fundamental period (Fig. 13e), the relative error is approximately 30%. Considering the simplicity and accuracy, the proposed model is suitable for practical seismic design. In addition, recent studies (Chandra et al. 2016; Guéguen et al. 2019) have shown the bias between nonlinear soil response from the experimental (in-situ) observation and numerical analysis, thus the proposed analytical model should be further validated and discussed using experimental data in future studies.

6 Conclusions

This study proposes a new analytical RSR model that considers the effect of earthquake scenarios. The mechanism of the effect of earthquake scenarios, i.e., the variation in the RSR with the earthquake scenario is systematically investigated by comparing it with the scenario-independent FSR based on random vibration theory. Using the proposed RSR model, the design spectrum incorporating site effects can be appropriately constructed. The main conclusions of this study can be summarized as follows:

1. The RSR varies with the earthquake scenario even for linear analysis, and the key factor governing the effect of earthquake scenarios is the ground-motion frequency content.
2. The overall shape of the RSR is similar to that of the FSR, their maximum values occur at the same period, and the maximum value of the FSR consistently exceeds that of the RSR.
3. The values of the RSR and FSR are similar at long periods, and the RSR values at long periods gradually approach those of the FSR with increasing magnitude and distance.
4. The values of the RSR and FSR at very short periods are very different, and the difference increases with increasing magnitude and distance.
5. The proposed RSR model is verified by comparing it with results obtained from SHAKE analysis while considering a variety of actual soil conditions. It was found that using the proposed model can derive good estimations of the design spectrum incorporating site effects.

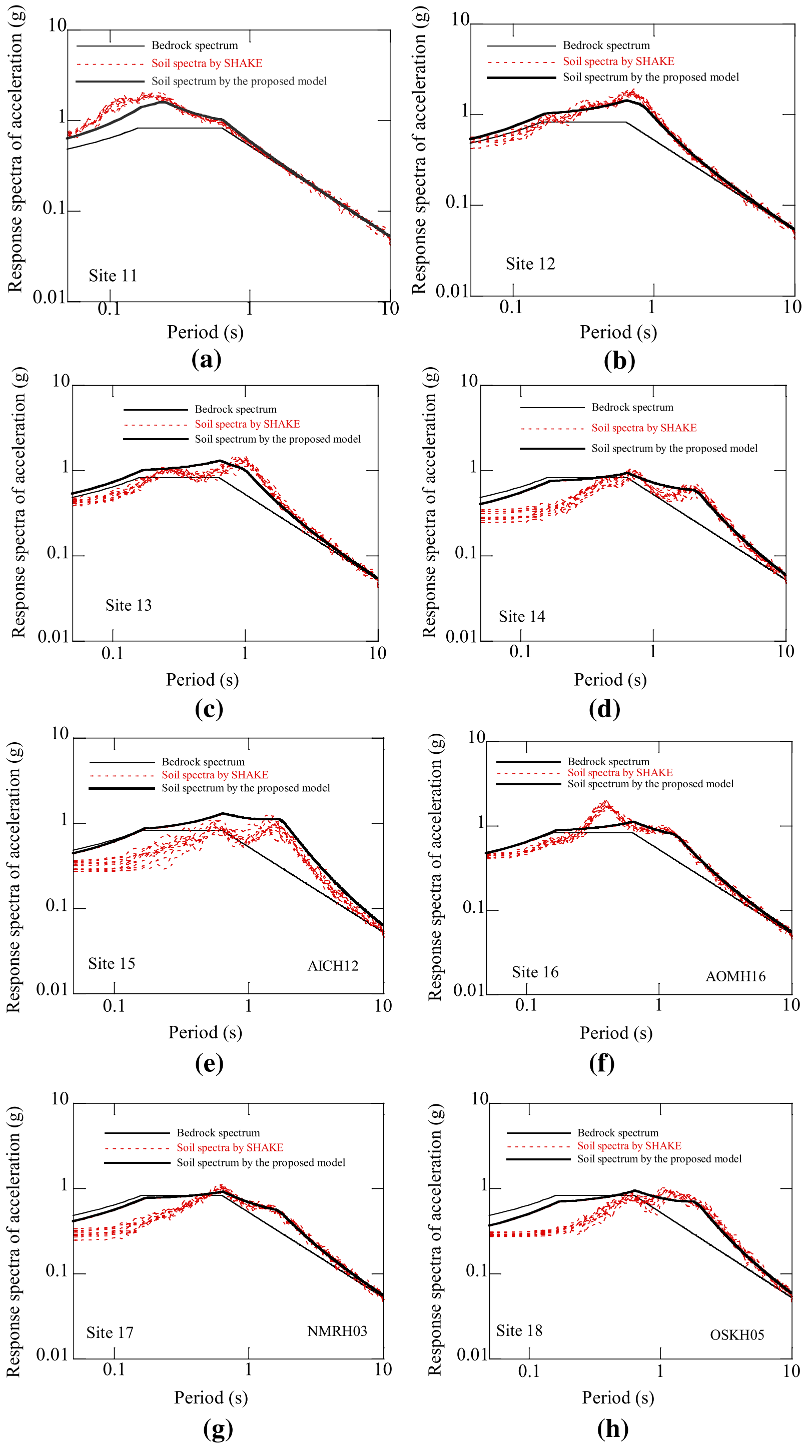

Fig. 13 Comparison of response spectra by the proposed model and SHAKE program **a** site 11, **b** site 12, **c** site 13, **d** site 14, **e** site 15, **f** site 16, **g** site 17, and **h** site 18

Acknowledgements This study was partially supported by the National Natural Science Foundation of China (Grant No. 51738001). The authors are grateful for the support.

Authors' contributions HZ: conceptualization, methodology, writing-original draft preparation, investigation. Y-GZ: data curation, visualization, supervision, writing-reviewing and editing.

Funding The research leading to these results received funding from the National Natural Science Foundation of China (Grant No. 51738001).

Data availability All data generated or analyzed during this study are included in this published article.

Code availability Available upon request.

Declarations

Conflict of interest The authors have no conflicts of interest to declare that are relevant to the content of this article.

References

Atkinson GM, Boore DM (1995) Ground motion relations for eastern north America. Bull Seism Soc Am 85:17–30

Atkinson GM, Silva W (2000) Stochastic modeling of California ground motions. Bull Seism Soc Am 90:255–274

ASCE/SEI 7-10 (2011) Minimum design loads for buildings and other structures. Structural Engineering Institute, American Society of Civil Engineers

Boore DM (1983) Stochastic simulation of high-frequency ground motions based on seismological models of the radiated spectra. Bull Seism Soc Am 73:1865–1894

Boore DM (2003) Simulation of ground motion using the stochastic method. Pure Appl Geophys 160:635–676

Boore DM (2005). SMSIM—Fortran programs for simulating ground motions from earthquakes: version 2.3, U.S. Geol. Surv. Open-File Rept. 2005 OFR 96-80-A, Menlo Park, California

Boore DM, Joyner WB (1997) Site amplifications for Generic Rock Sites. Bull Seism Soc Am 87:327–341

Boore DM, Thompson EM (2012) Empirical improvements for estimating earthquake response spectra with random-vibration theory. Bull Seism Soc Am 102:761–772

Boore DM, Thompson EM (2015) Revisions to some parameters used in stochastic-method simulations of ground motion. Bull Seism Soc Am 105:1029–1041

Bora SS, Scherbaum F, Kuehn N, Stafford PJ (2016) On the relationship between Fourier and response spectra: implications for the adjustment of empirical ground-motion prediction equations (GMPEs). Bull Seis Soc Am 106:1235–1253

Borcherdt RD (1994) Estimates of site-dependent response spectra for design (methodology and justification). Earthq Spectra 10:617–653

Cartwright DE, Longuet-Hlggms MS (1956) The statistical distribution of the maxima of a random function. Proc R Soc Lond A 237:212–223

Chandra J, Gueguen P, Bonilla LF (2016) PGA-PGV/Vs considered as a stress–strain proxy for predicting nonlinear soil response. Soil Dyn Earthq Eng 85:146–160

Davenport AG (1964) Note on the distribution of the largest value of a random function with application to gust loading. Pro Inst Civ Eng 28:187–196

Dobry R (1991) Soil properties and earthquake response, 1171–1187, IV, Proceeding of X European Conference of Soil Mechanics and Foundation Engineering; 26–30 May, 1991, Florence, Italy

Dobry R, Borcherdt RD, Crouse CB, Idriss IM, Joyner WB, Martin GR, Power MS, Rinne EE, Seed RB (2000) New site coefficients and site classification system used in recent building seismic code provisions. Earthq Spectra 16:41–67

European Committee for Standardization CEN (2004). Eurocode 8: design of structures for earthquake resistance—part 1: general rules, seismic actions and rules for buildings, European Standard EN 1998-1

Frankel A, Mueller C, Barnhard T, Perkins D, Leyendecker E, Dickman N, Hanson S, Hopper M (1996) national seismic hazard maps: documentation June 1996. U.S Geol Surv Open-File Rept 69:96–532

Guéguen P, Bonilla LF, Douglas J (2019) Comparison of soil nonlinearity (*In situ* stress-strain relation and $G/G_{\max}$ reduction) observed in strong-motion databases and modeled in ground-motion prediction equations. Bull Seism Soc Am 109(1):178–186

Idriss IM, Sun JI (1992) SHAKE91: A computer program for conducting equivalent linear seismic response analyses of horizontally layered soil deposits. University of California, Davis, User's Guide

Inoue W, Hayashi Y, Arai H, Nakai S, Iiba M (2010) A study on method to evaluate seismic amplification ratios of surface strata. AIJ J Technol Des 16:107–112 **(in Japanese)**

International Building Code (IBC) (2012). Country Club Hill, Illinois, USA: International Code Council

Japanese Seismic Design Code (2000). Technical Standard for Structural Calculation of Response and Limit Strength of Buildings. Notification No.1457–2000, Ministry of Land, Infrastructure and Transport **(in Japanese)**

Kozo Keikaku Engineering Inc. ARTEQ, program for generating artificial earthquake motions, Japan

Kottke AR, Rathje EM (2008) Technical manual for Strata. University of California, Berkeley

Kottke AR, Rathje EM (2013) Comparison of time series and random-vibration theory site-response methods. Bull Seism Soc Am 103:2111–2127

Koyamada K, Miyamoto Y, Tokimatsu K, Miura K (2004) Practical evaluation for soil response and pile stress in a liquefiable site using response spectrum method. AIJ J Technol Des 19:47–52 **(in Japanese)**

Liu L, Pezeshk S (1999) An improvement on the estimation of pseudoresponse spectral velocity using RVT method. Bull Seism Soc Am 89:1384–1389

Lam NTK, Wilson JL, Chandler AM (2001) Seismic displacement response spectrum estimated from the analogy soil amplification model. Eng Struct 23:1437–1452

Park D, Hashash YMA (2004) Soil damping formulation in nonlinear time domain site response analysis. J Earthq Eng 08(02):249–274

Rosenblueth E, Arciniega A (1992) Response spectral ratios. Earthq Eng Struct Dyn 21:483–492

Régnier J, Bonilla LF, Bertrand E, Semblat JF (2014) Influence of the V_S profiles beyond 30 m depth on linear site effects: assessment from the KiK-net data. Bull Seism Soc Am 104(5):2337–2348

Stafford PJ, Rodriguez-Marek A, Edwards B, Kruiver P, Bommer JJ (2017) Scenario dependence of linear site effect factors for short-period response spectral ordinates. Bull Seism Soc Am 107:2859–2872

Strong-motion Seismograph Networks (K-NET, KIK-net). http://www.kyoshinbosai.go.jp/kyoshin/. Accessed 16 Sept 2020

Tsang HH, Adrian MC, Lam NTK (2006) Estimating non-linear site response by single period approximation. Earthq Eng Struct Dyn 35:1053–1076

Tsang HH, Wilson JL, Lam NTK, Su RKL (2017) A design spectrum model for flexible soil sites in regions of low-to-moderate seismicity. Soil Dyn Earthq Eng 92:36–45

Vanmarcke EH (1975) On the distribution of the first-passage time for normal stationary random processes. J Appl Mech 42:215–220

Wang X, Rathje EM (2016) Influence of peak factors on site amplification from random vibration theory based site-response analysis. Bull Seism Soc Am 106:1–14

Zhang HZ, Zhao YG (2018) A simple approach for estimating the first resonance peak of layered soil profiles. J Earthq Tsunami 12:185005

Zhang HZ, Zhao Y (2019) A simple approach for estimating the fundamental mode shape of layered soil profiles. J Earthq Tsunami 13:1950003

Zhang HZ, Zhao Y (2021) Investigation of relationship between the response and Fourier spectral ratios based on statistical analyses of strong motion records. J Earthq Tsunami 2150008

Zhao JX, Zhang J, Kojiro I (2009) Side effect of using response spectral amplification ratios for soil sites-variability and earthquake-magnitude and source-distance dependent amplification ratios for soil sites. Soil Dyn Earthq Eng 29:1262–1273

Zhao JX, Zhang J (2010) Side-effect of using response spectral amplification ratios for soft soil sites—earthquake source-type dependent amplification ratios. Soil Dyn Earthq Eng 30:258–269